Research Square

Preprints are preliminary reports that have not undergone peer review.
They should not be considered conclusive, used to inform clinical practice,
or referenced by the media as validated information.

Characterization of the complete plastomes of two flowering epiparasites (Phacellaria glomerata and P. compressa, Santalaceae, Santalales): gene content, organization and plastome degradation

Xiaorong Guo
Yunnan University
Changkun Liu
Kunming Institute of Botany Chinese Academy of Sciences
Hengchang Wang
Wuhan Botanical Garden
Guangfei Zhang
Yunnan University
Hanjing Yan
Guangdong Pharmaceutical University
Wenhua Su
Yunnan University
Yunheng Ji (jiyh@mail.kib.ac.cn)
Institute of Botany Chinese Academy of Sciences https://orcid.org/0000-0002-1116-7485

Research article

Keywords: Epiparasitism, parasitic plants, Phacellaria compressa, Phacellaria glomerata, plastome degradation, Santalaceae, Santalales

Posted Date: April 24th, 2019

DOI: https://doi.org/10.21203/rs.2.9317/v1

License: This work is licensed under a Creative Commons Attribution 4.0 International License.
Read Full License

Abstract

Backgrounds: The transition to a heterotrophic lifestyle triggers reductive evolution of plastid genome (plastome) in both photosynthetic and non–photosynthetic parasites. A plant parasite parasitizing another plant parasite is referred to as epiparasitism, which is extremely rare in angiosperms. In despite of the particularly special lifeform of epiparasitic plants, their plastomes have not been characterized to date. Sequending such plastomes may enable new insights into the evolutionary pathway of plastome degradation associated with parasitism. Results: In this study, we generated complete plastomes of Phacellaria compressa and P. glomerata (Santalaceae, Santalales) through Illumina shotgun sequencing. Plastome assembly and comparison indicated that plastomes of both species exhibit the quadripartite structure typical of angiosperms, and that they possess similar size, structure, gene content, and arrangement of genes to other hemiparasites in Santalales, especially to those hemiparasites in Santalaceae. The plastomes of P. compressa and P. glomerata were characterized by the functional loss of plastid–encoded NAD(P)H–dehydrogenase and infA genes, which strongly coincides with the general pattern of plastome degradation observed in Santalales hemiparasites. Conclusion: Our study demonstrates that the shift to epiparasitism and reduced vegetative bodies in P. compressa and P. glomerata do not appear to cause any unique plastome degradation compared with their closely related hemiparasites. The epiparasitic lifestyle or an endophytic growth form observed in these two epiparasites may have limited impact on the reductive modification of their plastomes.

Background

Chloroplast, with essential roles in photosynthesis, is an organelle in plant cells that contains its own genome, the plastome [1]. As a result of long evolutionary processes, plastomes have been subjected to strong selective pressures that tend to maintain conservatism in terms of genome size, structure, gene content, and organization [2]. Nevertheless, the lifestyle shift from autotrophy to heterotrophy in plants (parasitism or mycoheterotrophy) is generally accompanied by progressively relaxed purifying selection in plastomes [3,4], and therefore results in significant modification of plastomes, including pseudogenization, gene loss, structural rearrangement, and size reduction [3–12].

Parasitism in plants is one of the outcomes of the transition from autotrophy to heterotrophy, involving a decrease or complete loss of photosynthetic capacity, and acquisition of nutrition and water from hosts [13]. It is estimated that parasitism has independently evolved at least 11 or 12 times in angiosperms [14, 15], and there are approximately 4,500 parasitic plants found in 20 families of flowering plants [13]. Parasitic plants are categorized as either hemiparasites (photosynthetic parasites) or holoparasites (nonphotosynthetic parasites). Hemiparasites possess varying degrees of photosynthetic capacity and only obtain some of their nutrients from host plants, while holoparasites have entirely lost their photosynthetic capacity and acquire all of their nutrients from host plants [13]. Such variable reliance on photosynthesis exerts different intensities of selective pressures on plastomes [3, 7]. As a result, plant parasites often possess plastomes with varying degrees of degeneration, ranging from partial or complete loss of plastid–encoded NAD(P)H–dehydrogenase (NDH) complex in hemiparasitic plants [7,

10, 16–19] to the functional loss of many photosynthesis–associated and energy production genes [7,11,20–26], or even the complete loss of plastomes [27] in holoparasitic plants.

A plant parasite parasitizing another plant parasite is termed as epiparasitism [28], hyperparasitism [29], secondary parasitism [30], or double parasitism [31]. This phenomenon is extremely rare in angiosperms, which has only been found in a few species (27 species to date) in Santalales [32]. It is noteworththt that all known epiparasites are capable of photosynthesis [13], they are thus regarded as a kind of paricularly special hemiparasitim [29]. Because of the rarity, the epiparasitic plastomes have remained uncharacterized to date.

Among known epiparasitic plants, about one third of the species belong to the genus *Phacellaria* [32] (Santalaceae, Santalales [33]). *Phacellaria* is found in the tropical and subtropical areas of Southeast Asia, and consists of eight species that mainly parasitize Loranthaceae hemiparasites [34]. Although all *Phacellaria* species are capable of photosynthesis, their vegetative bodies grow endophytically in the parasitic host [34]. This growth form in hemiparasites may represent a transitional stage in the evolution toward holoparasitism [13]. Characterization of the plastomes of *Phacellaria* species may enable insights into the evolution of plastomes associated with the lifestyle shift from hemiparasitism to holoparasitism. In addition, the epiparasitic lifestyle and the reduced vegetative bodies observed in *Phacellaria* species mean a greater reliance on host plants for nutrients [29]. Given that a previous study suggested that the varying nutritional dependences on host may influence the plastome evolution in hemiparasites [16], the comparison of plastome features and degree of platome degradation with their hemiparasitic relatives can offer information in elucidating whether a higher level of nutritional reliance on the host plants in *Phacellaria* species leads to a higher level of plastome degradation.

In this study, two epiparasites, namely, *Phacellaria compressa* and *P. glomerata* were sampled for Illumina shotgun sequencing. Specifically, we aimed to: (1) assemble and characterize their complete plastomes;(2) compared the plastomes among representatives of Santalales in order to gain insights into the reductive evolution of plastome associated with parasitism; (3) examine whether the epiparasitic lifestyle and the reduced vegetative bodies leads to some unique plastome degradation in both species.

Methods

Plant sampling and genome shotgun sequencing

Specimens of *P. compressa* and *P. glomerata* (Fig. 1) were collected from Tengchong Country, Yunnan Province, China. Vouchers (*P. compressa*: L. F. Yang 005; *P. glomerate*: L. F. Yang 013; identified by Dr. Yunheng Ji) were preserved in the herbarium of Kunming Institute of Botany, Chinese Academy of Sciences (KUN). The collection of the samples completely complies with local and national legislation permission. Tissue samples were collected and dried with silica gel for DNA extraction. Genomic DNA was extracted from *ca.* 50 mg of tissue using a modified CTAB method [35]. Approximately 5μg of purified genomic DNA was sheared by sonication. Paired–end libraries with an average insert size 350 bp

were prepared using a TruSeq DNA Sample Prep Kit (Illumina, Inc., USA) according to the manufacturer's protocol. Libraries were sequenced using the Illumina HiSeq 2500 system at BGI (Wuhan, Hubei, China).

Plastome assembly, annotation and comparison

Raw Illumina reads were filtered by NGS QC tool kit [36] to remove adaptors and low–quality reads. The trimmed reads were assembled into contigs with SPAdes v3.10.1 [37]. The representative plastid contigs were extracted and checked using BLAST searches against the reference plastome of *Dendrotrophe varians* (MF592987). The position and direction of each contig was manually adjusted according to the reference plastome using Geneious V10.2 [38]. The resulting plastomes were annotated using the Dual Organellar Genome Annotator database [39], by carrying out BLAST searches of all plastid genes against the assembled plastomes. Protein–coding genes with one or more frameshift mutations or premature stop codons were regarded as pseudogenes. Start and stop codons and intron/exon boundaries for protein–coding genes were checked manually. Genes putatively annotated as transfer RNA (tRNA) were further verified by tRNAscan–SE 1.21[40] using default parameters.

To date, a total of 14 plastomes in Santalales (**Additional file 1**) have been published [16,17,19,41–44], including an autotrophic species, *Erythropalum scandens* (Erythropalaceae), as well as 13 hemiparasites, namely, *Helixanthera parasitica*, *Macrosolen cochinchinensis*, *Taxillus chinensis*, *T. sutchuenensis* (Loranthaceae), *Champereia manillana* (Opiliaceae), *Dendrotrophe varians*, *Osyris alba*, *Viscum album*, *V. coloratum*, *V. crassulae,* and *V. minimum* (Santalaceae), *Schoepfia jasminodora* (Schoepfiaceae), and *Malania oleifera* (Ximeniaceae). In order to compare the plastome structure, gene content, and arrangement of *Phacellaria* plastomes with relative species in the order Santalales, these publicly available plastomes were downloaded from the NCBI GenBank database. Gene content, as well as the IRs/LSC and IRs/SSC boundaries among multiple plastomes in Santalales were compared using Geneious V10.2 [38]. To examine the structural shift in platomes, whole plastome alignment among Santalales hemiparasites was performed with Mauve v 2.3.o [45]. The autotrophic species, *E. scandens* was used as the reference for ProgressiveMauve analysis.

Phylogenetic analysis

In order to investigate the relationships of *P. compressa* and *P. glomerata* within Santalales, their plastomes together with all published Santalales plastomes (**Additional file 1**) were included in the phylogenomic analysis. *Haloxylon persicum* (Amaranthaceae, Caryophyllales) was employed as an outgroup. The alignment of plastomes was made using MAFFT [46], and manually edited where necessary. Phylogenetic analyses consisted of standard maximum likelihood (ML) and Bayesian inference (BI) methods. ML analysis was reconstructed using RAxML–HPC BlackBox version 8.1.24 [47] with 1,000 replicates of rapid bootstrap (BS) under the GTRCAT model. The best substitution model (GTR + I + G) for BI analysis was selected using the program Modeltest v3.7 [48] with the Akaike information criterion [49]. BI was performed with MRBAYES v.3.1.2 [50], and the posterior probability values (PP) were

run with trees sampling every 100 generations for one million total generations, with the first 25% discarded as burn–in. Stationarity was considered to be reached when the average standard deviation of split frequencies was less than 0.01. Phylogenetic trees were presented and edited using FigTree version 1.4.2 [51].

Results

Plastome size and structure

The complete plastome of *P. compressa* and *P. glomerata* was 138,903 bp and 138,684 bp in length (**Fig. 2**). The sequencing coverage for each plastome was 464.074 × and 696.985 × (**Additional file 2**), which confirmed the accuracy and reliability of the *de novo* plastome assembly of the two epiparasites. The fully assembled and annotated plastomes of *P. compressa* and *P. glomerata* were deposited in the NCBI GanBank database under the accession number MK387848 and MK387849. Both species exhibited the typical quadripartite structure, which consists of a pair of inverted repeat regions (IRs) separated by the large single copy (LSC) region and the small single copy (SSC) region (**Fig. 2**). Features of the *P. compressa* and *P. glomerata* plastomes were presented in **Table 1**. By comparison with the published plastomes of hemiparasitic plants in Santalales [16,17,19,41–44], the size of the complete plastome, LSC, and IR in *P. compressa* and *P. glomerata* was similar to that of *Champereia manillana*, *Dendrotrophe varians* and *Osyris alba*, whilst slightly larger than that of the remaining species in the order (**Table 1**). As an obvious SSC reduction was observed in *C. manillana*, the SSC size of *P. compressa* and *P. glomerate* was closer to that of *O. alba* and *D. varians*. The plastomes of *P. compressa* and *P. glomerata* had a similar GC content (37.9%), which was unevenly distributed in LSC, SSC, and IRs. The highest GC content was found in the IR regions, followed by LSC. The lowest GC content was observed in the SSC region.

The junctions of IR/SSC and IR/LSC of plastomes in Santalales are divergent (**Fig. 3**). The SSC region in *Malania oleifera* had been extremely contracted, such that no genes are included. The IRb/SSC boundaries of most species fell into the *ycf1* gene, but moved to the intergenic regions of *trnN_GUU–ycf1* in *D. varians*, *O. alba*, *P. compressa,* and *P. glomerata*. The junction of IRa/SSC included *ndhF* in *E. scandens*, *ccsA* in *O. alba*, *trnL–UAC* in species from Loranthaceae (*M. cochinchinensis*, *T. chinensis*, *T. sutchuenensis*, *H. parasitica*), and the intergenic region of *trnN_GUU–rpl32* in the remaining species. Four types of IR/LSC boundaries were observed in Santalales plastomes. The *Viscum* species had the most expanded IR/LSC boundaries, in which the gene *rpl22* was duplicated. IR expansions in *C. manillana*, *D. varians*, *O. alba*, *P. compressa,* and *P. glomerata* duplicated the *rps19* gene. The IR regions of *E. scandens* and *M. oleifera*, as well as species belonging to Loranthaceae, expanded into the *rpl2* gene. The IR/LSC junctions of *S. jasminodora* were located between *trnL–CAA* and *ycf2*.

Gene loss and pseudogenization

The plastomes of *P. compressa* and *P. glomerata* identically encoded a total of 101 potentially functional genes, including 67 protein–coding genes, 30 tRNA genes, and four ribosomal RNA genes (**Table 2**). Both species have completely lost 10 plastid NAD genes, namely, *ndhA*, *C*, *D*, *E*, *F*, *G*, *H*, *I*, *J*, and *K*. We also found that *ndhB* and *infA* had been pseudogenized in both species. By comparison with reported plastomes in Santalales, the gene content (intact genes) of *P. compressa* and *P. glomerata* plastomes was highly identical to that of *C. manillana*, *D. varians,* and *O. alba*, and very similar to that of *Viscum* species (**Additional file 2 & 3**).

In Santalales, the nonparasitic plant *E. scandens* had retained all plastid–encoded *ndh* genes, whereas physical loss or pseudogenization of *ndh* genes had been detected in all parasitic plants (**Additional file 2**). Also, the physical or functional loss of *infA* was also shared in parasites except for *S. jasminodora* (**Additional file 2 & 3)**. Consisting of only 80 genes, *M. oleifera* possesses the most degenerated plastome in Santalales, in which the genes encoding photosystem subunits (*psaC*, *psbA*, *I*, *K*, *L* and *M*), cytochrome *b*6*f* complex (*petB*), *ccsA*, maturase K (*matK*), and *ycf1* had been deleted. Except for *M. oleifera*, the loss or pseudogenization of these genes had not been observed in any other Santalales hemiparasites.

Phylogenetic relationships

Tree topologies based on ML and BI phylogeny were identical to each other (**Fig. 4**). The 16 species in Santalales were recovered as four major clades with high support values. The autotrophic species *E. scandens* (Erythoropalaceae) and the root hemiparasite, *M. oleifera* (Ximeniaceae) were resolved as two basally diverged clades, and the remaining species formed two fully supported clades (MS=100%, PP=1.0). Within the first clade (MS=100%, PP=1.0), *S. jasmiodora* (root hemiparasitism, Schoepfiaceae) was sister to species of Loranthaceae (stem hemiparasitism). Within the second clade (MS=100%, PP=1.0), the sister relationship between Opliaceae (*C. manillana*, root hemiparasitism) and Santalaceae was recovered. The relationships recovered by our data were highly congruent with previous studies using single or multiple DNA sequences with a more extensive taxon sampling of Santalales, which suggested that root hemiparasitism is the ancestral state in contrast to stem hemiparasitism [52,53].

Discussion

Plastome structure and gene content

Santalales consists of 18 families, approximately 160 genera and 2,200 species [53], which comprises almost half of all known parasitical angiosperms, but also includes a relatively small number of autotrophic species in Erythropalaceae, Strombosiacae, and Coulaceae [13,52–54]. It is notable that the reported platomes represent only a small portion of the diversity in the order. Nevertheless, comparison of plastome features among autotrophic, hemiparasitic, and epiparasitic Santalales may provide useful clues for addressing whether epiparasitism influences the plastome evolution in the studied species.

A typical angiosperm plastome possesses 113 genes, including 79 protein–coding genes, 30 tRNA genes and four ribosomal RNA genes [2]. In Santalales, only the autotrophic *E. scandens* plastome contains a relatively complete gene content, which encodes 112 genes, consisting of 79 protein–coding genes, 29 tRNA genes and four rRNA genes [44]. With functional gene totals ranging from 80 to 101 in *P. compressa*, *P. glomerata*, and other Santalales hemiparasites [16,17,19,41–44], a size reduction compared to typically autotrophic angiosperms occurred in these hemiparasitic platomes, which made the plastome size of *P. compressa* and *P. glomerata*, as well as the hemiparasites in Santalales, slightly smaller than that of *E. scandens* (**Table 1 & 2**) and other autotrophic angiosperms. Similar levels of gene loss had been found in other hemiparasitic plants [7,10,18].

Despite *P. compressa* and *P. glomerata* exhibiting an epiparastic lifestyle, and their vegetative tissues largely reduced, they likely retained the capacity for photosynthesis because their bodies were overall green [34]. Notably, both *P. compressa* and *P. glomerata*, as well as *C. manillana*, *D. varians*, *O. alba*, and *S. jasminodora* maintained more functional genes than other Santalales hemiparasites (**Table 2**). The data suggest that the epiparasitic lifestyle and even the endophytic habitat of *P. compressa* and *P. glomerata* have not resulted in further gene loss compared with their hemiparasitic relatives. It is interesting to note that the content of intact genes in *P. compressa* and *P. glomerata* plastomes is identical to that of *C. manillana*, *D. varians*, and *O. alba*, and very similar to that of *Viscum* species, which belong to the family Santalaceae (**Fig. 4, Additional file 2 & 3**). This implies that functional gene loss in Santalales parasitic plants may occur in a highly lineage–specific manner.
IR expansion and contraction often result in size variations in angiosperm plastomes, leading to the lineage–specific gain or loss of a small number of genes in these regions [55,56]. However, large–scale IR expansions and contractions were only observed in a few autotrophic angiosperms [56]. By comparison, this phenomenon seems to be more common in parasitic plants. For instance, the holoparasite *Cytinus hypocistis* (Cytinaceae, Malvales) has lost each IR region [25]. Additionally, the IR has been reduced to 1,466 bp in the holoparasite *Hydnora visseri* (Hydnoraceae, Piperales) [24]. A significant IR contraction to the intergenic spacer between *ycf2* and *trnL–CAA* has been observed in the plastome of a hemiparasite in Santalales, *S. jasminodora* (Schoepfiaceae) [19]. On the other hand, large IR expansions have been observed in the holoparasite *Cynomorium coccineum* (Cynomoriaceae, Saxifragales) [57], and hemiparasitic *Striga* species (Orobanchaceae, Lamiales) [10]. Taken together, these findings suggest that dramatic IR shifts not only occur in holoparasites but also in hemiparasites. However, the similarity of the IR size in *P. compressa* and *P. glomerata* to that of most hemiparasitic species in Santalales implies that the epiparasitic lifestyle of both species has not caused obvious structural changes in the plastomes of *P. compressa* and *P. glomerate*, as the result of Progressive Mauve Alignment indicated (**Additional file 4**).

Plastome degradation in Santalales hemiparasites

The plastid NDH complex mediates photosystem I cyclic electron transport and facilitates chlororespiration in plant cells [58]. The NDH complex is comprised of approximately 30 subunits. Of those, 11 subunits (*ndhA*, *B*, *C*, *D*, *E*, *F*, *G*, *H*, *I*, *J*, and *K*) are encoded by the plastome [59]. Functional and physical loss of these genes is commonly observed in parasitic plants, which is regarded as an early

response of plastomes in the evolution of a parasitic lifestyle [60]. Similar to the plastomes of previously studied hemiparasites in Santalales [16,17,19,41–44] and other angiosperm orders [7,10,18], both *P. compressa* and *P. glomerata* have functionally lost all plastid–encoded *ndh* genes, suggesting that the NDH complex is the only gene group that has been entirely lost (physically or functionally) from the plastomes of photosynthetic parasites. The results further confirm the assumption that in parasitic plants with photosynthetic capacity, the *ndh* pathway is not indispensable [10, 12, 61].

In Santalales parasites, *infA* is another commonly reduced gene. The functional loss of *infA* and other housekeeping genes from heterotrophic plastomes is one of the greatest enigmas in heterotrophy–associated plastome degeneration [12]. Nevertheless, the phenomenon has been observed in a wide diversity of autotrophic angiosperms [62]. As a result, *infA* has been regarded as one of the most mobile plastid genes in angiosperms, which are often transferred to and retained in the nucleus [62–64]. Accordingly, we assume that the transfer of *infA* from the plastome to the nuclear genome may occur in Santalales parasitic plants.

Despite the fact *M. oleifera* is a hemiparasite that maintains photosynthetic capacity, it is surprising to observe that *psa*, *psb*, and *pet* genes have been partially deleted from its plastome. To our knowledge, *M. oleifera* is the only hemiparasitic plant to date in which critical photosynthetic genes have been partially lost from the plastome. If hemiparasitism represents a transitional step toward the evolution of holoparasitism, this observation in *M. oleifera* indicate that the reduction or loss of such genes may occur at a rather early stage. On the other hand, the partial reduction of these genes from the *M. oleifera* plastome implies that degeneration of photosynthetic capacity may be a gradual process. This process may have initiated at the hemiparasitic stage and is not likely completed until a holoparasitic lifestyle is achieved [3,12].

Conclusion

Overall, the plastomes of the epiparasites *P. compressa* and *P. glomerata* possess similar size, gene content, and arrangement to other hemiparasites in Santalales, particularly to those phylogenetically–related hemiparasites. Our data reveal that plastome degradation in *P. compressa* and *P. glomerata* greatly coincides with general trends observed in photosynthetic parasites, that is the functional loss of the *ndh* pathway [12]. Moreover, the shift to epiparasitism and reduced vegetative bodies do not appear to result in further plastome degradation in *P. compressa* and *P. glomerata*. The study suggests that an epiparasitic lifestyle or an endophytic growth form may have limited impact on reductive plastome evolution in *P. compressa* and *P. glomerata*.

Abbreviations

BGI: Beijing Genomics Institute; BLAST: Basic Local Alignment Search Tool; CTAB: Cetyl trimethylammonium bromide; tRNA: Transfer RNA; LSC: Large single–copy; SSC: Small single copy; IR: Inverted repeat; NCBI: National Center for Biotechnology Information; ML: Maximum Likelihood; BI:

Bayesian Inference; BS: Bootstrap; MCMC: Markov Chain Monte Carlo; bp: Base pair; rRNA: Ribosomal RNA

Declarations

Ethics approval and consent to participate

Not applicable.

Consent for publication

Not applicable.

Availability of data and materials

The complete plastome sequences of *P. compressa* and *P. glomerata* were deposited in the NCBI GanBank database under the accession number MK387848 and MK387849. The raw data of illumina sequencing were submitted to NCBI under the accession number (SRR8712668). The data used in the analysis are included within the article and the additional file 1.

Competing Interests

The authors declare that the research was conducted in the absence of any commercial or financial relationships that could be construed as a potential conflict of interest.

Funding
The authors would like to thank the financial support from the Major Program of National Natural Science Foundation of China (31590823), the National Natural Science Foundation of China (31060052, 31872673), and the NSFC–Joint Foundation of Yunnan Province (U1802287) in design of the study, and collection, analysis and interpretation of data, as well as in writing the manuscript.

Author Contributions

YJ and XG designed the research; XG and CL collected and analyzed the data; YJ and XG wrote the manuscript. HW, HY, GZ and WS discussed the results and revised the manuscripts.

Acknowledgments

We are grateful to Zhangming Wang for his help in collecting samples used in the study, and to Lifang Yang, Jin Yang, Zhenyan Yang, and Zhijie Ruan for their assistant in data analysis.

Reference

1. Palmer JD. Comparative organization of chloroplast genomes. Annu. Rev. Genet. 1985; 19:325–354. doi: 10.1146/annurev.ge.19.120185.001545.

2. Wicke S, Schneeweiss GM, Depamphilis CW, Müller KF, Quandt D. The evolution of the plastid chromosome in land plants: gene content, gene order, gene function. Plant Mol. Biol. 2011; 76: 273–297. doi: 10.1007/s11103–011–9762–4.

3. Wicke S, Müller KF, Claude WD, Quandt D, Bellot S, Schneeweiss GM. Mechanistic model of evolutionary rate variation en route to a nonphotosynthetic lifestyle in plants. Proc. Natl. Acad. Sci. USA. 2016; 113:9045–9050. doi: 10.1073/pnas.1607576113.

4. Barrett CF, Wicke S, Sass C. Dense infraspecific sampling reveals rapid and independent trajectories of plastome degradation in a heterotrophic orchid complex. New Phytol. 2018; 218:1192–1204. doi: 10.1111/nph.15072.

5. Depamphilis CW, Palmer JD. Loss of photosynthetic and chlororespiratory genes from the plastid genome of a parasitic flowering plant. Nature. 1990; 348:337–339. doi: 10.1038/348337a0.

6. Wolfe KH, Morden CW, Palmer JD. Function and evolution of a minimal plastid genome from a nonphotosynthetic parasitic plant. Proc. Natl. Acad. Sci. USA. 1992; 89:10648–10652. doi: 10.1073/pnas.89.22.10648

7. Wicke S, Muller KF, De Pamphilis CW, Quandt D, Wickett NJ, Yan Z, et al. Mechanisms of Functional and Physical Genome Reduction in Photosynthetic and Nonphotosynthetic Parasitic Plants of the Broomrape Family. Plant Cell. 2013; 25:3711–3725. doi: 10.1105/tpc.113.113373.

8. Feng YL, Wicke S, Li JW, Han Y, Lin CS, Li DG, et al. Lineage–specific reductions of plastid genomes in an orchid tribe with partially and fully mycoheterotrophic species. Genome Biol. Evol. 2016; 8: 2164–2175. doi: 10.1093/gbe/evw144.

9. Braukmann TW, Broe MB, Stefanović S, Freudenstein JV. On the brink: the highly reduced plastomes of nonphotosynthetic Ericaceae. New Phytol. 2017; 216: 254–266. doi: 10.1111/nph.14681.

10. Frailey DC, Chaluvadi SR, Vaughn JN, Goatney CG, Bennetzen JL. Gene loss and genome rearrangement in the plastids of five Hemiparasites in the family Orobanchaceae. BMC Plant Biol. 2018; 18: 30. doi: 10.1186/s12870–018–1249–x.

11. Schneider AC, Chun H, Stefanović S, Baldwin BG. Punctuated plastome reduction and host–parasite horizontal gene transfer in the holoparasitic plant genus Aphyllon. Proc. R. Soc. B. 2018; 285: 20181535. doi: 10.1098/rspb.2018.1535.

12. Wicke S, Naumann J. Molecular evolution of plastid genomes in parasitic flowering plants. Adv. Bot. Res. 2018; 85: 315–347. doi: 10.1016/bs.abr.2017.11.014

13. Heide–Jørgensen H. Parasitic flowering plants. Brill, 2008.

14. Barkman TJ, Mcneal JR, Lim SH, Coat G, Croom HB, Young ND, et al. Mitochondrial DNA suggests at least 11 origins of parasitism in angiosperms and reveals genomic chimerism in parasitic plants. BMC Evol. Biol. 2007; 7: 248–0. doi: 10.1186/1471–2148–7–248.

15. Westwood JH, Yoder JI, Timko MP, De Pamphilis CW. The evolution of parasitism in plants. Trends Plant Sci. 2010; 15: 0–235. doi: 10.1016/j.tplants.2010.01.004.

16. Petersen G, Cuenca A, Seberg O. Plastome Evolution in Hemiparasitic Mistletoes. Genome Biol. Evol. 2015; 7: 2520–2532. doi: 10.1093/gbe/evv165.

17. Li Y, Zhou JG, Chen XL, Cui YX, Xu ZC, Li YH, et al. Gene losses and partial deletion of small single–copy regions of the chloroplast genomes of two hemiparasitic *Taxillus* species. Sci. Rep. 2017; 7: 12834. doi: 10.1038/s41598–017–13401–4

18. Wu CS, Wang TJ, Wu CW, Wang YN, Chaw SM. Plastome evolution in the sole hemiparasitic genus laurel dodder (*Cassytha*) and insights into the plastid phylogenomics of Lauraceae. Genome Biol. Evol. 2017; 9: 2604–2614. doi: 10.1093/gbe/evx177.

19. Shin HW, Lee NS. Understanding plastome evolution in Hemiparasitic Santalales: Complete chloroplast genomes of three species, *Dendrotrophe varians*, *Helixanthera parasitica*, and *Macrosolen cochinchinensis*. PLoS ONE. 2018; 13. doi: 10.1371/journal.pone.0200293

20. Delavault PM, Russo NM, Lusson NA, Thalouarn PA. Organization of the reduced plastid genome of *Lathraea clandestina*, an ahlorophyllous parasitic plant. Physiol. Plant. 1996; 96: 674–682. doi: 10.1111/j.1399–3054.1996.tb00242.x.

21. Nickrent DL, Ouyang Y, Duff RJ, De Pamphilis CW. Do nonasterid holoparasitic flowering plants have plastid genomes? Plant Mol. Biol. 1997; 34: 717–729. doi: 10.1023/A:1005860632601.

22. Mcneal JR, Kuehl JV, Boore JL, De Pamphilis CW. Complete plastid genome sequences suggest strong selection for retention of photosynthetic genes in the parasitic plant genus *Cuscuta*. BMC Plant Biol. 2007; 7: 57–0. doi: 10.1186/1471–2229–7–57.

23. Bellot S, Renner SS. The plastomes of two species in the endoparasite genus *Pilostyles* (Apodanthaceae) each retain just five or six possibly functional genes. Genome Biol. Evol. 2015; 8: 189–201. doi: 10.1093/gbe/evv251.

24. Naumann J, Der JP, Wafula EK, Jones SS, Wagner ST, Honaas LA, et al. Detecting and Characterizing the Highly Divergent Plastid Genome of the Nonphotosynthetic Parasitic Plant *Hydnora visseri* (Hydnoraceae). Genome Biol. Evol. 2016; 8: 345–363 doi: 10.1093/gbe/evv256.

25. Roquet C, Coissac E, Cruaud C, Boleda M, Boyer F, Alberti A, et al. Understanding the evolution of holoparasitic plants: the complete plastid genome of the holoparasite, *Cytinus hypocistis*, (Cytinaceae). Ann. Bot. 2016; 118: 885–896. doi: 10.1093/aob/mcw135.

26. Samigullin TH, Logacheva MD, Penin AA, Vallejo–Roman CM. Complete Plastid Genome of the Recent Holoparasite *Lathraea squamaria* Reveals Earliest Stages of Plastome Reduction in Orobanchaceae. PLoS ONE. 2016; 11: e0150718. doi: 10.1371/journal.pone.0150718.

27. Molina J, Hazzouri KM, Nickrent D, Geisler Mattew, Meyer RS, Pentong MM, et al. Possible Loss of the Chloroplast Genome in the Parasitic Flowering Plant *Rafflesia lagascae* (Rafflesiaceae). Mol. Biol. Evol. 2014; 31: 793–803. doi: 10.1093/molbev/msu051.

28. Visser JH. Epiparasitism–how many mistletoes on one another. The Golden Bough (Royal Botanic Gardens, Kew). 1982; 1: 4.

29. Mathiasen RL, Nickrent DL, Shaw DC, Watson DM. Mistletoes: Pathology, Systematics, Ecology, and Management. Plant Dis. 2008; 92: 988–1006. doi: 10.1094/PDIS–92–7–0988.

30. Liddy J. Dispersal of Australian mistletoes: the Cowiebank study. The Biology of Mistletoes, Academic Press, Sydney. 1983; pp. 101–116.

31. Martin, W. The flora of New Zealand. pp. Whitcombe and L. Tombs Ltd., Christchurch.1961; pp. 101–116.

32. Wilson CA, Calvin CL. Metadata provide insights on patterns of epiparasitism in mistletoes (Santalales), an overlooked topic in forest biology. Botany. 2017: 95: 259–269. doi: 10.1139/cjb–2016–0264.

33. Angiosperm Phylogeny Group. An update of the Angiosperm Phylogeny Group classification for the orders and families of flowering plants: APG IV. Bot. J. Lin. Soc. 2016; 181:1–20.

34. Li D. Distribution, present situation and conservation strategy of the genus *Phacellaria.* Biodivers. Sci. 2005; 13: 262–268. doi: 10.1360/biodiv.040204.

35. Doyle JJ. A rapid DNA isolation procedure for small quantities of fresh leaf tissue. Phytochem Bull.1987; 19: 11–15.

36. Patel RK, Mukesh J. NGS QC Toolkit: A Toolkit for Quality Control of Next Generation Sequencing Data. PLoS ONE. 2012; 7: e30619. doi: 10.1371/journal.pone.0030619.

37. Nurk S, Bankevich A, Antipov D, Gurevich AA. Korobeynikov A. Lapidus A, et al. Assembling Single–Cell Genomes and Mini–Metagenomes From Chimeric MDA Products. J. Comput. Biol. 2013; 20: 714–737. doi: 10.1089/cmb.2013.0084.

38. Kearse M, Moir R, Wilson A, Cheung M, Sturrock S, Buxton S, et al. Geneious Basic: An integrated and extendable desktop software platform for the organization and analysis of sequence data. Bioinformatics. 2012; 28: 1647–1649. doi: 10.1093/bioinformatics/bts199.

39. Wyman SK, Jansen RK, Boore JL. Automatic annotation of organellar genomes with DOGMA. Bioinformatics. 2004; 20: 3252–3255. doi: 10.1093/bioinformatics/bth352.

40. Schattner P, Brooks AN, Lowe TM. The tRNAscan–SE, snoscan and snoGPS web servers for the detection of tRNAs and snoRNAs. Nucleic Acids Res. 2005; 33 (Web Server issue):W686–9. doi: 10.1093/nar/gki366.

41. Su HJ, Hu JM. The complete chloroplast genome of hemiparasitic flowering plant *Schoepfia jasminodora*. Mitochondr DNA Part B. 2016; 1: 767–769 doi: 10.1080/23802359.2016.1238753.

42. Yang GS, Wang YH, Wang YH, Shen SK. The complete chloroplast genome of a vulnerable species *Champereia manillana* (Opiliaceae). Conserv. Genet. Res. 2017; 9: 415–418. doi: 10.1007/s12686–017–0697–1.

43. Liu SS, Hu YH, Maghuly F, Porth IM, Mao JF. The complete chloroplast genome sequence annotation for *Malania oleifera*, a critically endangered and important bioresource tree. Conserv. Genet. Res. 2018. 1–4. doi: 10.1007/s12686–018–1005–4.

44. Zhu ZX, Wang JH, Cai YC, Zhao KK, Moore MJ, Wang HF. Complete plastome sequence of *Erythropalum scandens* (Erythropalaceae), an edible and medicinally important liana in China. Mitochondr DNA Part B. 2018; 3:139–140. doi: 10.1080/23802359.2017.1413435.

45. Darling AE, Mau B, Perna NT. ProgressiveMauve: multiple genome alignment with gene gain, loss and rearrangement. PLoS One. 2010; 5: e11147.

46. Katoh K, Standley DM. MAFFT Multiple Sequence Alignment Software Version 7: Improvements in Performance and Usability. Mol. Biol. Evol. 2013; 30: 772–780. doi: 10.1093/molbev/mst010.

47. Stamatakis A. RAxML–VI–HPC: maximum likelihood–based phylogenetic analyses with thousands of taxa and mixed models. Bioinformatics. 2006; 22: 2688–2690. doi: 10.1093/bioinformatics/btl446.

48. Posada D, Crandall KA. MODELTEST: testing the model of DNA substitution. Bioinformatics. 1998; 14: 817–818. doi: 10.1093/bioinformatics/14.9.817.

49. Posada D, Buckley TR. Model selection and model averaging in phylogenetics: advantages of Akaike information criterion and Bayesian approaches over likelihood ratio tests. Syst. biol. 2004; 53: 793–808. doi: 10.1080/10635150490522304.

50. Ronquist F, Huelsenbeck JP. MrBayes 3: Bayesian phylogenetic inference under mixed models. Bioinformatics. 2003; 19: 1572–1574. doi: 10.1093/bioinformatics/btg180.

51. Rambaut A: FigTree v1.4.2. 2014; University of Edinburgh, Edinburgh. [http://beast.bio.ed.ac.uk/figtree]

52. Der JP, Nickrent DL. A Molecular Phylogeny of Santalaceae (Santalales). Syst. Bot. 2008; 33: 107–116. doi: 10.1600/036364408783887438.

53. Nickrent DL, Malécot V, Vidal–Russell R, Der JP. A revised classification of Santalales. Taxon. 2010; 59: 538–558. doi: 10.2307/25677612.

54. Nickrent DL. Plantas parásitas de la Península Ibérica e Islas Baleares. Madrid: Mundi–Prensa Libros, 2002: 7–27.

55. Plunkett GM, Downie SR. Expansion and contraction of the chloroplast inverted repeat in Apiaceae subfamily Apioideae. Syst. Bot. 2000; 25:648–667.doi: 10.2307/2666726.

56. Chumley TW, Palmer JD, Mower JP, Calie PJ, Boore JL, Jansen RK. The complete chloroplast genome sequence of *Pelargonium x hortorum*: Or ganization and evolution of the largest and most highly rearranged chloroplast genome of land plants. Mol. Biol. Evol. 2006; 23: 2175–2190. doi: 10.1093/molbev/msl089.

57. Bellot S, Cusimano N, Luo S, Sun G. Zarre S, Temsch E, et al. Assembled plastid and mitochondrial genomes, as well as nuclear genes, place the parasite family Cynomoriaceae in the Saxifragales. Genome Biol. Evol. 2016; 8: 189-201. doi: 10.1093/gbe/evw147.

58. Yamori W, Shikanai T. Physiological Functions of Cyclic Electron Transport Around Photosystem I in Sustaining Photosynthesis and Plant Growth. Annu. Rev. Plant Biol. 2016; 67: 67: 81–106. doi: 10.1146/annurev–arplant–043015–112002.

59. Friedrich T, Klaus Steinmüller, Weiss H. The proton–pumping respiratory complex I of bacteria and mitochondria and its homologue in chloroplasts. FEBS Lett. 1995; 367: 107–111. doi: 10.1016/0014–5793(95)00548–N.

60. Funk H T, Berg S, Krupinska K, Maier UG, Krause K. Complete DNA sequences of the plastid genomes of two parasitic flowering plant species, *Cuscuta reflexa* and *Cuscuta gronovii*. BMC Plant Biol. 2007; 7: 45–0. doi: 10.1186/1471–2229–7–45.

61. Lin CS, Chen JJW, Chiu CC, Hsiao HCW, Yang CJ, Jin XH, et al. Concomitant loss of NDH complex–related genes within chloroplast and nuclear genomes in some orchids. Plant J. 2017; 90: 994–1006. doi: 10.1111/tpj.13525.

62. Millen RS, Olmstead RG, Adams KL, Palmer JD, Lao NT, Tony LH, et al. Many parallel losses of *infA* from chloroplast DNA during angiosperm evolution with multiple independent transfers to the nucleus. Plant Cell. 2001; 13: 645–658. doi: 10.2307/3871412.

63. Ahmed I, Biggs PJ, Matthews PJ, Collins LJ, Hendy MD, Lockhart PJ. Mutational dynamics of aroid chloroplast genomes. Genome Biol. Evol. 2012; 4: 1316–1323. doi: 10.1093/gbe/evs110

64. Liu LX, Li R, Worth J R P, Li X, Li P, Cameron KM, et al. The Complete Chloroplast Genome of Chinese Bayberry (*Morella rubra*, Myricaceae): Implications for Understanding the Evolution of Fagales. Front. Plant Sci. 2017; 8: 968. doi: 10.3389/fpls.2017.00968.

Tables

Table 1. Comparision of plastome features among 16 Santalales species

Species	Plastome		LSC		IR		SSC	
	Size (bp)	GC content (%)	Size(bp)	GC content (%)	Size(bp)	GC content (%)	Size(bp)	GC content (%)
Phacellaria compressa	138,903	37.9	80,099	35.6	24,104	43.6	10,596	29.5
Phacellaria glomerata	138,684	37.9	79,937	35.6	24,080	43.6	10,587	29.6
Viscum minimum	131,016	36.2	75,814	33.3	23,094	43.2	9,014	24.2
Viscum crassulae	126,064	36.4	73,226	33.6	22,105	43.4	8,628	24.0
Viscum album	128,921	36.4	73,893	33.5	23,198	43.2	8,632	24.8
Viscum coloratum	128,744	36.3	73,684	33.4	23,215	43.1	8,630	24.3
Osyris alba	147,253	37.7	84,601	35.6	24,340	43.1	13,972	31.2
Schoepfia jasminodora	118,743	38.1	84,168	36.1	12,406	47.9	9,763	30.7
Champereia manillana	147,461	37.4	83,505	35.3	28,075	41.9	7,806	27.9
Taxillus chinensis	121,363	37.3	70,357	34.7	22,462	43.0	6,082	26.2
Taxillus sutchuenensis	122,562	37.3	70,630	34.7	22,915	42.8	6,102	26.2
Erythropalum scandens	156,154	38.0	84,799	36.2	26,394	42.8	18,567	32.3
Helixanthera parasitica	124,881	36.5	73,043	33.8	22,752	42.3	6,334	25.5
Macrosolen cochinchinensis	122,986	36.6	69,018	33.6	23,912	42.2	6,144	24.4
Dendrotrophe varians	140,666	37.8	81,684	35.5	24,056	43.7	10,870	29.7
Malania oleifera	125,050	38.2	76,387	35.0	24,324	43.2	15	40.0

Table 2. Summary of gene content (potentially functional genes) among 16 Santalales plastomes

Species	Plastid genes	Protein-coding genes	rRNA	tRNA
Phacellaria compressa	101	67	4	30
Phacellaria glomerata	101	67	4	30
Viscum minimum	99	66	4	29
Viscum crassulae	98	66	4	28
Viscum album	96	64	4	28
Viscum coloratum	96	64	4	28
Osyris alba	101	67	4	30
Schoepfia jasminodora	99	68	4	27
Champereia manillana	100	66	4	30
Taxillus chinensis	90	63	4	23
Taxillus sutchuenensis	90	63	4	23
Erythropalum scandens	113	79	4	30
Helixanthera parasitica	92	63	4	25
Macrosolen cochinchinensis	92	63	4	25
Dendrotrophe varians	101	67	4	30
Malania oleifera	77	52	4	21

Additional File Legend

Additional file 1: GenBank accessions of plastomes examined in this study.

Additional file 2: Comparison of gene content among 16 Santalales plastomes.

Additional file 3: Comparison of plastome structure, gene content and organization of *Phacellaria compressa* and *P. glomerata* with other Santalales species, with phylogenetic relationships indicated.

Additional file 4: Progressive Mauve alignment of 16 Santalales plastomes. The order of plastomes, from top to bottom, is *Phacellaris compress*, *P. glomerata*, *Dendrotrophe varians*, *Osyris alba*, *Champereia manillana*, *Viscum minimum*, *V. crassulae*, *V. crassulae*, *V. album*, *V. coloratum*, *Schoepfia jasminodora*, *Taxillus chinensis*, *T. sutchunenensis*, *Helixanthera parasitica*, *Macrosolen cohinchinensis*, *Malania oleifera*, *Erythropalum sandens*.

Figures

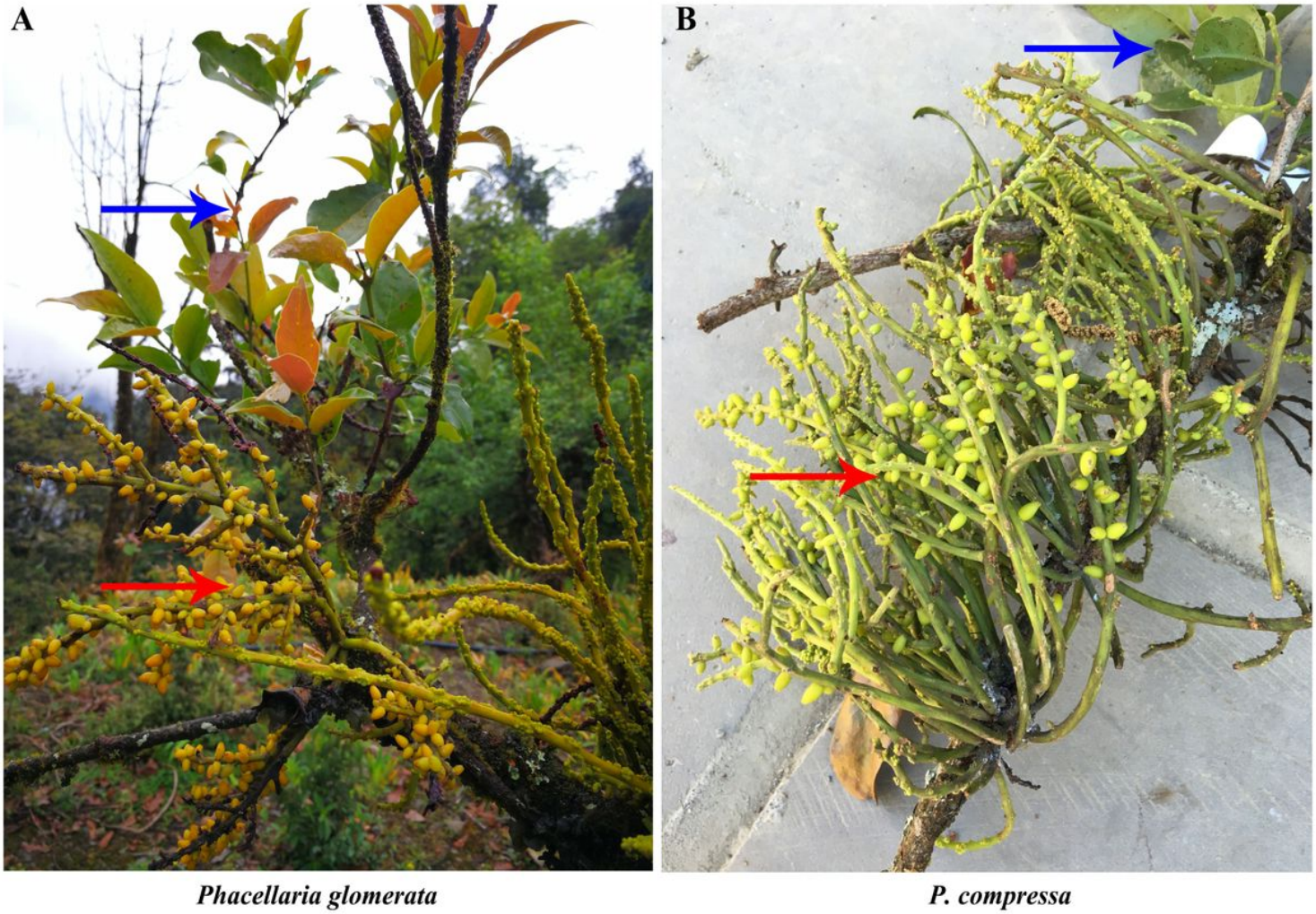

Figure 1

The epiparasitic lifestyle and endophytic growth form of two Phacellaria specie. (A) P. glomerata (red arrow) growing on the stem hemiparasite, Taxillus sericus (blue arrow); (B) P. compressa (red arrow) growing on the stem hemiparasite, Dendrophthoe pentandra (blue arrow).

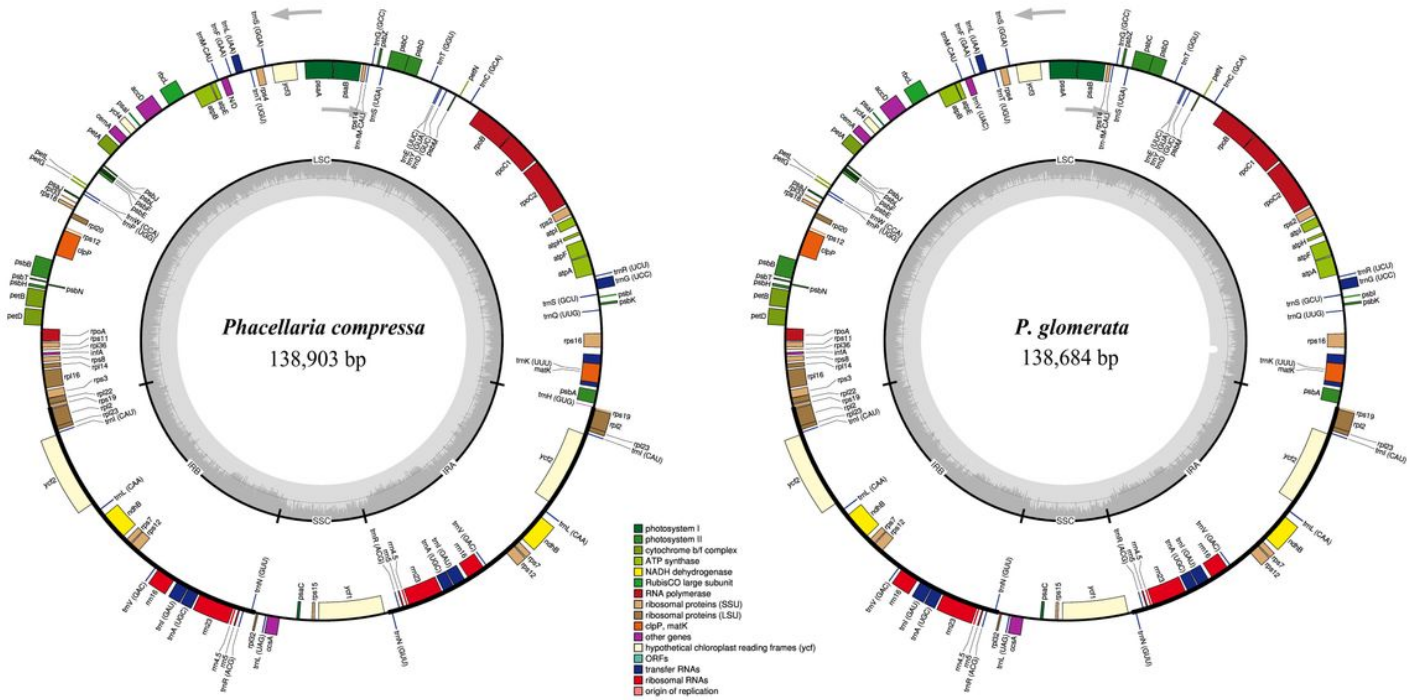

Figure 2

Plastome maps of Phacellaria compressa and P. glomerata. Genes shown outside the circle are transcribed clockwise, and those inside are transcribed counterclockwise. The dark gray area in the inner circle indicates the CG content of the plastome.

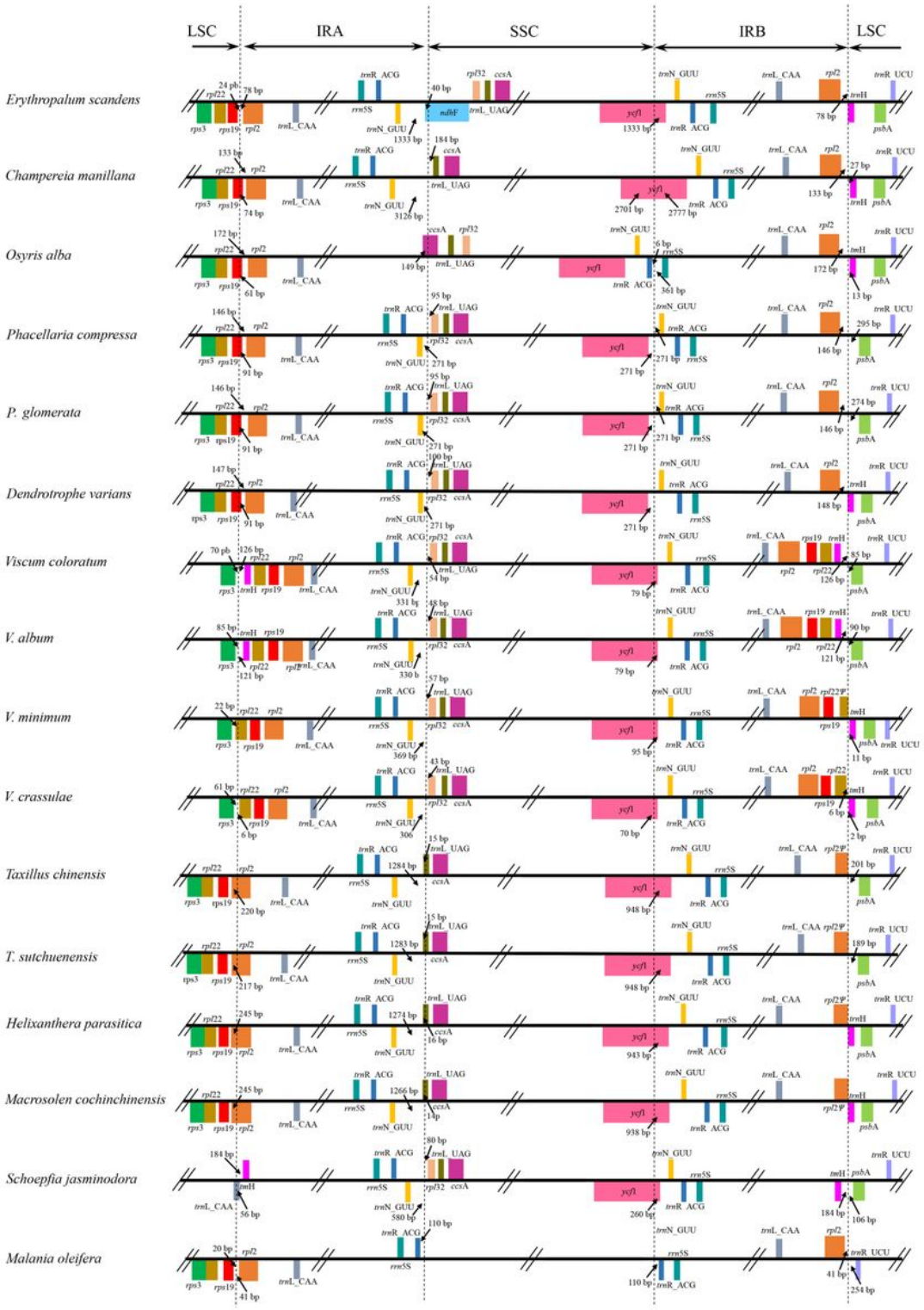

Figure 3

IR expansion and contraction dynamics among 16 Santalales plastomes.

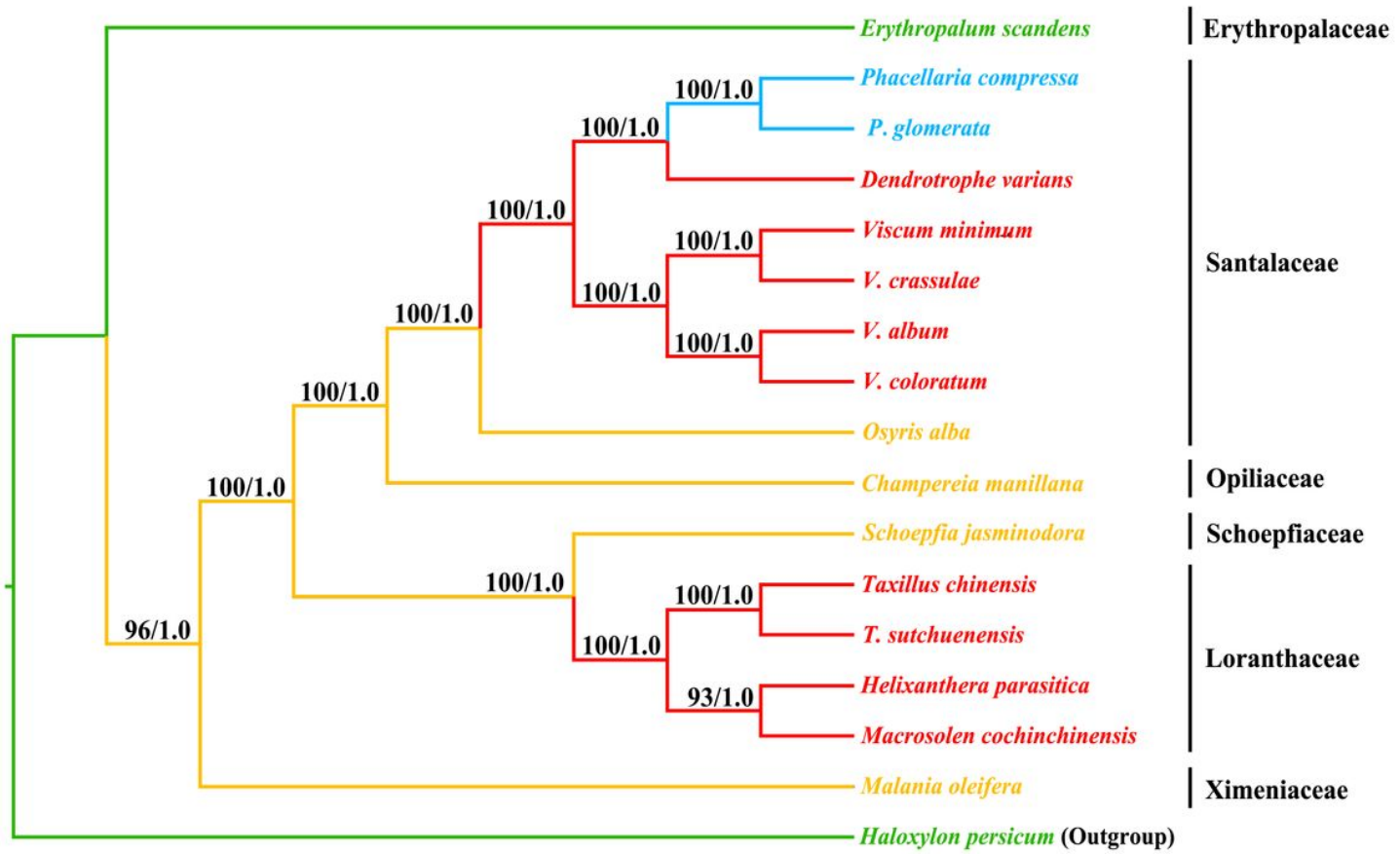

Figure 4

Phylogenetic relationships of Phacellaria compressa and P. glomerata to other Santalales species. Based on the tree topology, the lifestyle evolution in Santalales is inferred. Numbers above the tree branches represent bootstrap (BS)/ posterior probability (PP) values. Green lineages: autotrophism; yellow lineages: root hemiparasitism; red lineages: stem hemiparasitism; blue lineages: epiparasitism.

Supplementary Files

This is a list of supplementary files associated with this preprint. Click to download.

- Additionalfile3.jpg
- Additionalfile2.xlsx
- Additionalfile4.pdf
- Additionalfile1.doc